radiation

MDPI

Article

Molecular and Cellular Responses to Ionization Radiation in Untransformed Fibroblasts from the Rothmund–Thomson Syndrome: Influence of the Nucleo-Shuttling of the ATM Protein Kinase

Joëlle Al-Choboq [1,†], Myriam Nehal [1,†], Laurène Sonzogni [1], Adeline Granzotto [1], Laura El Nachef [1], Juliette Restier-Verlet [1], Mira Maalouf [2], Elise Berthel [1], Bernard Aral [3], Nadège Corradini [4], Michel Bourguignon [1,5] and Nicolas Foray [1,*]

[1] Inserm, U1296 Unit, Radiation: Defense, Health and Environment, Centre Léon-Bérard, 28 rue Laennec, 69008 Lyon, France
[2] Department of Chemistry and Biochemistry, Faculty of Sciences II, American University, 2611 Fanar, Lebanon
[3] Centre Hospitalo, Universitaire Dijon Bourgogne, 21070 Dijon, France
[4] Institut d'hématologie et d'oncologie pédiatrique, Centre Léon-Bérard, 28 rue Laennec, 69008 Lyon, France
[5] Department of Biophysics and Nuclear Medicine, Université Paris Saclay (UVSQ), 78035 Versailles, France
* Correspondence: nicolas.foray@inserm.fr; Tel.: +33-4-78-78-28-28
† These authors contributed equally to this work.

Simple Summary: The molecular and cellular radiosensitivity associated with the Rothmund–Thomson syndrome has been investigated in the framework of a mechanistic model based on the radiation-induced nucleo-shuttling of the ATM protein.

Abstract: The Rothmund–Thomson syndrome (RTS) is a rare autosomal recessive disease associated with poikiloderma, telangiectasias, sun-sensitive rash, hair growth problems, juvenile cataracts and, for a subset of some RTS patients, a high risk of cancer, especially osteosarcoma. Most of the RTS cases are caused by biallelic mutations of the *RECQL4* gene, coding for the RECQL4 DNA helicase that belongs to the RecQ family. Cellular and post-radiotherapy radiosensitivity was reported in RTS cells and patients since the 1980s. However, the molecular basis of this particular phenotype has not been documented to reliably link the biological and clinical responses to the ionizing radiation (IR) of cells from RTS patients. The aim of this study was therefore to document the specificities of the radiosensitivity associated with RTS by examining the radiation-induced nucleo-shuttling of ATM (RIANS) and the recognition and repair of the DNA double-strand breaks (DSB) in three skin fibroblasts cell lines derived from RTS patients and two types derived from RTS patients' parents. The results showed that the RTS fibroblasts tested were associated with moderate but significant radiosensitivity, a high yield of micronuclei, and impaired DSB recognition but normal DSB repair at 24 h likely caused by a delayed RIANS, supported by the sequestration of ATM by some RTS proteins overexpressed in the cytoplasm. To our knowledge, this report is the first radiobiological characterization of cells from RTS patients at both molecular and cellular scales.

Keywords: Rothmund–Thomson syndrome; radiosensitivity; DNA double-strand breaks; ATM; ionizing radiation

Citation: Al-Choboq, J.; Nehal, M.; Sonzogni, L.; Granzotto, A.; El Nachef, L.; Restier-Verlet, J.; Maalouf, M.; Berthel, E.; Aral, B.; Corradini, N.; et al. Molecular and Cellular Responses to Ionization Radiation in Untransformed Fibroblasts from the Rothmund–Thomson Syndrome: Influence of the Nucleo-Shuttling of the ATM Protein Kinase. *Radiation* **2023**, *3*, 21–38. https://doi.org/10.3390/radiation3010002

Academic Editor: Michael Hausmann

Received: 16 December 2022
Revised: 14 January 2023
Accepted: 16 January 2023
Published: 18 January 2023

1. Introduction

Rothmund–Thomson syndrome is a rare disease discovered jointly by a German ophthalmologist, Auguste Rothmund, and an English dermatologist, Sydney Thomson. In 1868, Rothmund associated skin rash and juvenile cataracts in some of his patients [1].

From 1921, Thomson named "poikiloderma congenitale" all of the erythema associated with the symptoms that Auguste Rothmund had described but also noticed that the erythema can be accompanied by some bone impairments [2]. Finally, in 1957, William Taylor made the fusion of both observations to integrate them in a more complete definition of a syndrome that he named the Rothmund–Thomson Syndrome (RTS) [3].

RTS is a skin disease characterized by poikiloderma, combining erythema and telangiectasia [4–9]. Poikiloderma does not appear at birth but approximately between the third and sixth month of life and spreads throughout the body (to the notable exception of the abdomen that is generally spared). In addition to these cutaneous features, RTS is also associated with sun-sensitive rash, nail and palmoplantar hyperkeratotic lesions, and dental alterations. The RTS patients present with short stature, sparse or absent hair, and juvenile cataracts [4–9]. In addition, RTS may be associated with bone or skin cancers. Such a difference in symptoms has generated the definitions of the following subsets: RTS type 1 (RTS1) is characterized by poikiloderma and early cataracts while RTS type 2 (RTS2) is marked by poikiloderma, congenital bone abnormalities (forehead bumps, concave nose) and a high risk of osteosarcomas in childhood and squamous cell carcinomas in later life [4]. The prevalence of RTS remains unknown. To date, about 500 RTS or RTS-like cases are described in the world. RTS affects double the amount of boys than girls. No specific treatment has been proposed to the RTS patients, which therefore implies a very low life expectancy (up to 20 years approximately) [4–9].

RTS is an autosomal recessive disease that has been associated with some mutations of the *RECQL4* gene that encodes the RECQL4 helicase protein [10,11] and with some mutations of the *ANAPC1* gene that encodes the anaphase promoting complex subunit 1 protein (ANAPC1) [12]. Conversely, some *RECQL4* mutations may be responsible for different syndromes: this is notably the case of the RAPADILINO [13] and Baller–Gerold [14] syndromes. It is also noteworthy that mutations of other helicases belonging to the same RECQ family as RECQL4 may cause other specific syndromes, such as Bloom syndrome (*RECQL2*/*BLM* mutations) and Werner syndrome (*RECQL3*/*WRN* mutations), both associated with accelerated aging [15,16]. Lastly, it is noteworthy that mutations of the other RECQ helicases, namely, RECQL and RECQL5, may affect viability so efficiently that no clinical syndrome has yet been associated (see Table 1 and references herein).

Table 1. The major genetic syndromes caused by mutations of RECQ helicases.

Syndrome	Gene Mutated	Protein	Clinical Features	References
Bloom	*RECQL2*/*BLM*	BLM helicase	Growth defect; Photosensitivity; Cancer predisposition	[17]
Werner	*RECQL3*/*WRN*	WRN helicase	Growth defect; Loss of hair; Cataracts; Skin atrophy; diabetes mellitus; atherosclerosis	[18]
Rothmund–Thomson	*RECQL4* *ANAPC1*	RECQL4 helicase ANAPC1	Poikiloderma; Short stature Dental abnormalities; Cataracts Risk of osteosarcomas for RTS2	[19]
RAPA-DILINO	*RECQL4*	RECQL4 helicase	RTS symptoms with Radial/Patellar hypoplasia; Cleft of Palate; Diarrhea; Dislocation joints; little size; Limb malformation; Slender Nose and Normal intelligence	[13]
Baller-Gerold	*RECQL4*	RECQL4 helicase	RTS symptoms with Craniosynostosis; Limb abnormality Thumb/radial hypoplasia	[14]

While the RTS patients may be exposed to ionizing radiation (IR) through radiodiagnosis for their clinical follow-up and eventually through radiotherapy to treat their tumor (for the RTS2 patients), the question of their radiosensitivity was raised in the 1980s: some authors investigated the radiobiological features of lymphocytes and fibroblasts from the RTS patients (Table 2 and references herein). In vitro clonogenic survival and cytogenetic features taken as endpoints or observations of post-radiotherapy reactions in healthy tissues suggest that RTS may be associated with a slight to moderate radiosensitivity. In parallel, a number of studies has aimed to elucidate the biological role of the RECQL4 protein in the DNA damage and signaling pathways, notably the management of the DNA double-strand breaks (DSB), the key-damage of the radiation-induced lethal effect [11,20–24]. However, most of these studies involved tumor or transformed fibroblast cell lines with very few cells from RTS donors. However, to reliably quantify the radiation-induced (RI) risks, i.e., the individual radiosensitivity (risk of post-radiotherapy tissue over-reactions), the radiosusceptibility (risk of RI cancer), and the radiodegeneration (risk of RI aging) of the RTS patients, represents a societal, medical, and scientific issue [25]. For example, in France, to evaluate the risks linked to the medical exposure to IR is inasmuch important as a recent governmental decree that recommends radiologists take into account the individual radiosensitivity and radiosusceptibility of their patients to justify irradiating acts [26].

Table 2. Non-exhaustive list of studies dealing with the radiobiological characterization of RTS cells.

RTS Cells/Donors	Techniques	Conclusions	Reference
4 fibroblasts cell lines	Cell survival DNA repair Repair replication	Significant radiosensitivity	[27]
1 fibroblast cell line	Cell survival	Slight radiosensitivity	[28]
1 fibroblast cell line	Colony formation	Enhanced Radiosensitivity But not toxicity to drugs	[29]
6 fibroblast cell lines	Colony formation	1.2 fold radiosensitivity	[30]
2 lymphocytes	G2 assay	Chromosomal radiosensitivity	[31]
1 patient		Clinical radiosensitivity after radiotherapy	[32]
1 patient		Clinical radiosensitivity after radiotherapy	[33]
3 fibroblast cell lines from RTS patients 2 fibroblast cell lines from RTS patients' parents	Cell survival Micronuclei γH2AX, pATM, MRE11 foci ATM-RECQL4 complexes	Moderate radiosensitivity Delayed RIANS	This study

Despite considerable efforts and a large spectrum of predictive assays, the quantification of the RI risks is still not consensual [34]. Since 2014, we have proposed a general and unified mechanistic model of the individual response to IR based on the RI ATM nucleo-shuttling (RIANS). The applications of the RIANS are numerous and concern both high- and low-dose phenomena. Particularly, the RIANS model may serve to predict radiosensitivity in a number of exposure conditions and was found relevant for more than twenty genetic diseases (e.g., [35–38]). To date, the RIANS model provides the highest statistically robust prediction of post-radiotherapy radiosensitivity [39–43] and a unified model to explain the linear–quadratic formula that links cell survival and dose [44]. More recently, we provided proof that assays using the RIANS biomarkers as endpoints are the most powerful molecular approaches to evaluate radiosensitivity with the clonogenic cell survival assay [45].

Here, by using successively clonogenic cell survival, micronuclei, and immunofluorescence assays with the RIANS biomarkers, we applied a routine procedure of radiobiological characterization [35,36,38,46–51] to document the individual molecular and cellular responses of fibroblast cell lines derived from three RTS patients and two of their relatives.

2. Materials and Methods

2.1. Cell Lines

All of the experiments were performed with untransformed fibroblast cells in the plateau phase of growth to avoid any cell cycle-dependent artifacts. Routine cell cytometry data indicated that 90–99% of cells were in G0/G1 phase [39,52]. Hence, the activity of the homologous recombination pathway during the experiments described here can be considered negligible [25]. Three radioresistant (1BR3, MRC5, and Hs27) controls that originated from radioresistant and apparently healthy patients and the hyper-radiosensitive *ATM*-mutated (AT4BI) and *LIG4*-mutated (180BR) cell lines were used in this study as negative and positive controls for radiosensitivity. These cell lines belong to the COPERNIC collection that has been abundantly documented and is composed of radioresistant, hyper-radiosensitive gifted cell lines and fibroblast cell lines derived from RT-treated patients. The COPERNIC database is protected under the reference IDDN.FR.001.510017.000.D.P.2014.000.10300. All sampling protocols of the COPERNIC collection were approved by the national ethical committee in agreement with the current national regulations. The resulting cells were declared under the numbers DC2008-585, DC2011-1437, and DC2021-3957 to the Ministry of Research. Three fibroblast cell lines from RTS patients were used (81CLB from the COPERNIC collection and AG17524 and AG18371 purchased from the Coriell Cell Repositories (Camden, NJ, USA)). Lastly, two fibroblast cell lines from RTS donor patients (AG18466 and AG18373), also purchased from the Coriell Cell Repositories, were also used in this study. Table 3 provides the major clinical and genetic features of all cell lines tested here.

Table 3. Non-exhaustive list of studies dealing with the radiobiological characterization of RTS cells.

Cell Lines	Origin	Syndrome	Genetic Features	Clinical Features
1BR3	COPERNIC	Apparently healthy	Apparently healthy	Apparently healthy radioresistance
MRC5	COPERNIC	Apparently healthy	Apparently healthy	Apparently healthy radioresistance
Hs27	COPERNIC	Apparently healthy	Apparently healthy	Apparently healthy radioresistance
AT4BI	COPERNIC	AT	*ATM* mutations	Hyper-radiosensitivity
180BR	COPERNIC	LIG4	LIG4 mutations	Hyper-radiosensitivity
81CLB	COPERNIC	RTS	Compound heterozygous *RTS* mutation t1:c.1236G > A, g.7844del	Severe poikiloderma; small stature, dental and bone abnormalities and diagnosed with epidermoid carcinoma and osteosarcoma at 17 years; died at 18
AG17524	Coriell Institute	RTS	Compound heterozygous *RTS* mutation g.2626(g.2626G > A) g.4644delAT	Skin rash at age 4 months; delayed tooth eruption; skin abnormalities; photosensitivity
AG18371	Coriell Institute	RTS	Homozygous RTS mutation g.2746(g.2746del11)	Diagnosed with osteosarcoma at age 11 years; died at 13; small

			g.2746(g.2746del11)	stature; severe poikiloderma; sparse eyebrows and eyelashes
AG18466	Coriell Institute	RTS donor parent Clinically unaffected	Heterozygous RTS mutation g.4503(g.4503C > T)	Female; 32 y; Clinically unaffected
AG18373	Coriell Institute	RTS donor parent Clinically unaffected	Heterozygous RTS mutation g.2746(g.2746del11)	Female; 42 y; Mother of AG18371 donor;

2.2. X-Ray Irradiation

Irradiations were performed with a 6 MeV photon medical irradiator (SL 15 Philips) (dose-rate: 6 $Gy.min^{-1}$) at the anti-cancer Centre Léon-Bérard (Lyon, France) [39,52]. The dosimetry features were certified by the radiophysics department of the Centre Léon-Bérard.

2.3. Zoledronate and Pravastatin Treatment (ZOPRA)

The combination (ZOPRA) of the anti-osteoporosis bisphosphonate (zoledronate) and the anti-cholesterol statin (pravastatin) was applied as described elsewhere [53]. Briefly, cells were incubated with 1 μM pravastatin (#P4498, Sigma–Aldrich France, Saint-Quentin-Fallavier, France) in Phosphatase-Buffered Saline (PBS) (#14040-091, Sigma–Aldrich) for 24 h at 37 °C; thereafter, 1 μM zoledronate (#SML0223, Sigma–Aldrich) in PBS was added to the culture medium for an additional 12 h at 37 °C [53].

2.4. Clonogenic Cell Survival Assay

The intrinsic cellular radiosensitivity was quantified from clonogenic cell survival data obtained from standard delayed plating procedures [54]. The survival data were fitted to the linear–quadratic (LQ) model that describes the cell survival S as a function of dose D, as follows:

$$S = e^{-(\alpha D + \beta D^2)} \quad (1)$$

where α and β are adjustable parameters to be determined [44].

2.5. Immunofluorescence

The immunofluorescence protocol and nuclear protein foci scoring were described elsewhere [38,39]. The polyclonal anti-rabbit anti-RECQL4 antibody (#PA5-55263, Invitrogen, Waltham, MS, USA) was used at 1:200. The anti-$\gamma H2AX^{ser139}$ antibody (#05-636; Merck Millipore, Burlington, USA) was used at 1:800. The monoclonal anti-mouse anti-*MRE11* (#56211) from QED Bioscience (San Diego, CA, USA) and the monoclonal anti-mouse anti-$pATM^{ser1981}$ (#05-740) from Merck Millipore were used at 1:100. Incubations with anti-mouse fluorescein (FITC) and rhodamine (TRITC) secondary antibodies were performed at 1:100 at 37 °C for 20 min. Slides were mounted in 4',6'Diamidino-2-Phényl-indole (DAPI)-stained Vectashield (Cliniscience, Nanterre, France) and examined with an Olympus BX51 fluorescence microscope.

2.6. Micronuclei Assay

During each immunofluorescence experiment, the DAPI counterstaining permits quantification of the micronuclei [55]. With such an approach, the micronuclei yield assessed is not numerically equivalent to that obtained with the micronucleus assay involving cytochalasin B [56]. Micronuclei data were expressed as the number of micronuclei per 100 cells (nuclei).

2.7. Proximity Ligation Assay

The proximity ligation assay (PLA) allows the visualization of endogenous protein–protein interactions at the single molecule level [57]; the protocol is detailed elsewhere [48]. The following antibodies were diluted in the Duolink antibody diluent 1X (#DUO82008, Sigma–Aldrich) at a ratio of 1:100: mouse monoclonal antibody (2C1 (1A1)) anti-*ATM* (#ab78), and rabbit monoclonal anti-*RTS* (#PA5-55263, Invitrogen). PLA foci were assessed as the number per cell.

2.8. Cell Extracts and Immunoblots

The procedures of the cell extracts and immunoblots are described elsewhere [48]. Briefly, total extracts were obtained with the (50 mM Tris, pH 8, 150 mM NaCl, 2 mM EDTA, pH 8, 10% glycerol, 0.2% Nonidet NP40, H_2O) lysis buffer. Cytoplasmic extracts were obtained with the (10 mM Hepes pH 7.9, 1.5 mM MgCl2, 10 mM KCL, 2 mM ethylenediaminetetraacetic acid (EDTA) pH 8, 0.5 mM dithiothreitol (DTT), 0.2% Nonidet NP40, H_2O) lysis buffer. Western blot bands were analyzed using ImageLab software (Bio-Rad Laboratories).

2.9. Statistical Analysis

Two-way ANOVA was used to compare two numerical values, and Spearman's test was used to compare the kinetic data. The foci kinetic data were fitted to the so-called Bodgi's formula that describes the kinetics for the appearance/disappearance of nuclear foci formed by some protein relocalization after irradiation [58]. Statistical analysis was performed by using Kaleidagraph v4 (Synergy Software, Reading, PA, USA) and Graphpad Prism (San Diego, CA, USA).

3. Results

3.1. Cellular Radiosensitivity of RTS Fibroblasts

The clonogenic cell survival at 2 Gy (SF2) is currently used to evaluate the cellular radiosensitivity [25,45,54,59]. The clonogenic survival assay was therefore applied to three RTS (81CLB, AG17524, GM18371), three radioresistant, and two hyper-radiosensitive fibroblast cell lines (Figure 1). The cellular radiosensitivity assessed in RTS fibroblasts was moderate but significant: the SF2 values of the three types of fibroblast cells were higher than those of radioresistant cells ($p < 0.001$) but lower than those of hyper-radiosensitive fibroblasts ($p < 0.0001$). The average SF2 value of the RTS fibroblasts was 22 ± 6% while the corresponding average values of the radioresistant and hypersensitive fibroblasts were 65 ± 3% and 2.5 ± 1.0%, respectively (Figure 1).

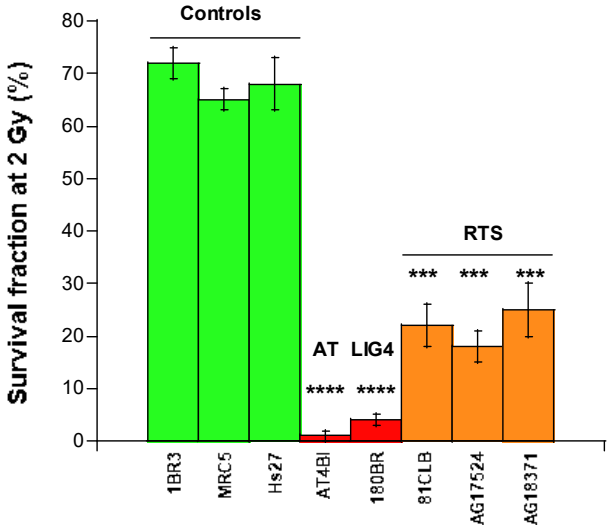

Figure 1. Clonogenic cell survival in RTS fibroblasts. Clonogenic cell survival assay was applied at 2 Gy to the radioresistant controls (1BR3, MRC5, Hs27), the hyper-radiosensitive *ATM*- (AT4BI) and *LIG4*- (180BR) mutated and the three RTS (81CLB, AG17524, AG18371) fibroblast cell lines. Each plot represents the mean ± SEM of at least two replicates. Asterisks represent statistical differences with radioresistant controls expressed as the *p*-value (3 and 4 asterisks correspond to $p < 0.001$ and $p < 0.0001$, respectively). AT: ataxia telangiectasia; LIG4: LIG4 syndrome.

3.2. Abnormally High Levels of Micronuclei in RTS Fibroblasts

The propagation of unrepaired DNA breaks up to mitosis may lead to irreversibly damaged chromosomal fragments causing mitotic death. Some chromosomal fragments may escape from the metaphases and generate micronuclei. Micronuclei have been shown to be quantitatively correlated with cellular radiosensitivity [25]. No significant difference was found between the spontaneous micronuclei in RTS cells and those in radioresistant controls ($p > 0.5$). Conversely, the number of spontaneous micronuclei per 100 cells was significantly higher in the two hyper-radiosensitive fibroblasts ($p < 0.02$). After 24 h post-irradiation, the number of residual micronuclei per 100 cells was significantly higher in the RTS fibroblasts ($p < 0.001$) compared with the radioresistant controls but lower than that observed in the hyper-radiosensitive fibroblasts ($p < 0.0001$) (Figure 2A), supporting a significant genomic instability in the RTS fibroblasts tested (Figure 2A). The average number of residual micronuclei per 100 cells was 13.3 ± 2.0 in the RTS fibroblasts while it was 55 ± 10 and 1.1 ± 0.5 in the hyper-radiosensitive and radioresistant control fibroblasts, respectively. The survival and micronuclei data from the three fibroblast cell lines were in full agreement with the correlation established between SF2 and micronuclei with fibroblasts from different genetic diseases and published recently [45] (Figure 2B).

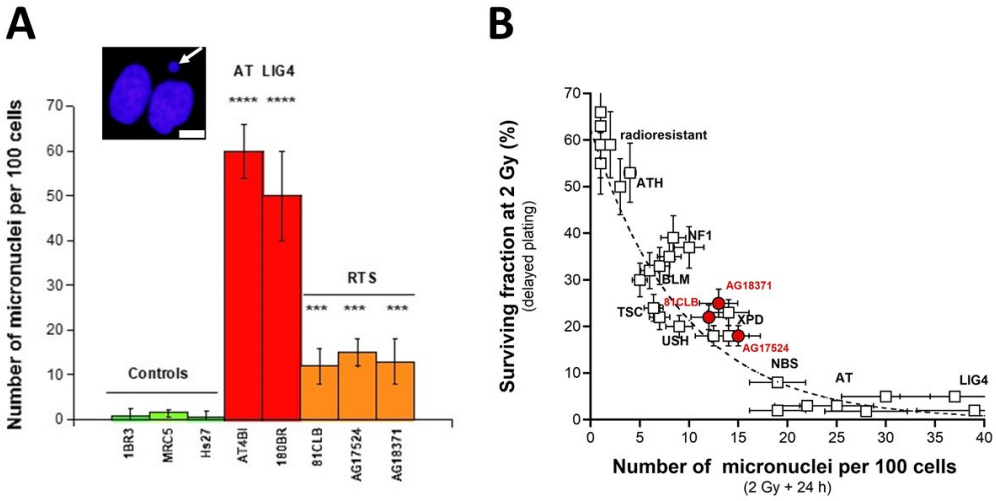

Figure 2. Micronuclei in RTS fibroblasts. (**A**). Number of micronuclei per 100 cells assessed 24 h after 2 Gy X-rays in the radioresistant controls (1BR3, MRC5, Hs27), the hyper-radiosensitive *ATM*- (AT4BI) and *LIG4*- (180BR) mutated, and the three RTS (81CLB, AG17524, AG18371) fibroblast cell lines. Each plot represents the mean ± SEM of three replicates. The insert shows a representative example of a micronucleus (white arrow) observed with DAPI counterstaining. The white bar corresponds to 5 µm. Asterisks represent statistical differences with radioresistant controls expressed as the *p*-value (3 and 4 asterisks correspond to $p < 0.001$ and $p < 0.0001$, respectively). AT: ataxia telangiectasia; LIG4: LIG4 syndrome. (**B**). With the use of historical data published in [45], the SF2 data and the corresponding micronuclei data from fibroblasts derived from the indicated syndromes (open squares) were plotted together (AT: ataxia telangiectasia, homozygous mutations of *ATM*; LIG4: homozygous mutations of *LIG4*; NBS: Nijmegen's syndrome, homozygous mutations of *NBS1*; XPD: xeroderma pigmentosum D, homozygous mutations of *XPD*; USH, Usher's syndrome, homozygous mutations of USH; TSC, tuberous sclerosis, heterozygous mutation of *TSC*; Bloom's syndrome, homozygous mutations of *BLM*; NF1, neurofibromatosis type 1, heterozygous

mutations of neurofibromin; ATH, heterozygous mutations of *ATM)*. The survival and micronuclei data from the RTS fibroblast cell lines shown in Figures 1 and 2A were added to the graph (red circles). The best data fit was obtained with a linear equation: SF2(%) = 62.2 exp(−0.107 MN_{24h}); r^2 = 0.939 (dotted line).

3.3. Abnormal Number of γH2AX Foci in RTS Fibroblasts after Irradiation

The micronuclei data suggest that a significant yield of DSB may remain unrepaired and participates in the lethal effect. To investigate the recognition and repair of radiation-induced DSB via the non-homologous end-joining (NHEJ) pathway, the most predominant DSB repair pathway in humans, we applied immunofluorescence to the phosphorylated form of the H2AX variant histone (γH2AX). According to the RIANS model, in response to radiation, cytoplasmic ATM dimers monomerize. The ATM monomers diffuse in the nucleus and phosphorylate the H2AX molecules at the DSB sites early after irradiation [43]. The ATM-dependent phosphorylation of H2AX histones is responsible for the formation of γH2AX foci reflecting the DSB recognized by *NHEJ*. Hence, the early γH2AX foci indicate the DSB recognition by NHEJ while the residual γH2AX foci reflect the unrepaired DSB among the DSB recognized by *NHEJ* [43]. Some spontaneous γH2AX foci were observed in the three fibroblast cell lines, but their number was not significantly different from that in the radioresistant controls ($p > 0.5$). In the radioresistant controls, the number of γH2AX foci scored 10 min after 2 Gy was 79 ± 4 per cell, consistent with the value 37 ± 4 per Gy per cell obtained in many situations [47]. The number of induced γH2AX foci scored 10 min post-irradiation in the three fibroblast cell lines was significantly lower than that in the radioresistant controls (81CLB: 40 ± 8; AG17524: 25 ± 4; AG18371: 22 ± 4 γH2AX foci per cell; $p < 0.001$) (Figure 3A). These findings suggest an impairment in the DSB recognition by NHEJ. It is noteworthy that the *ATM*-mutated AT4BI fibroblasts did not show any γH2AX foci while the *LIG4*-mutated 180BR fibroblasts elicited a slow γH2AX foci repair kinetic, reflecting a gross DSB repair defect, in full agreement with literature [37,39,45,47]. It must be stressed here that while ATR and DNA-PK kinases may phosphorylate H2AX, *ATR*- and *DNA-PKcs*-mutated cells show γH2AX foci early after irradiation whereas the great majority of *ATM*-mutated cells generally do not [60]. For example, the AT5BI cell lines may show less than 10 γH2AX foci at 10 min post-irradiation. Both AT4BI and AT5BI have been shown elsewhere [37,48].

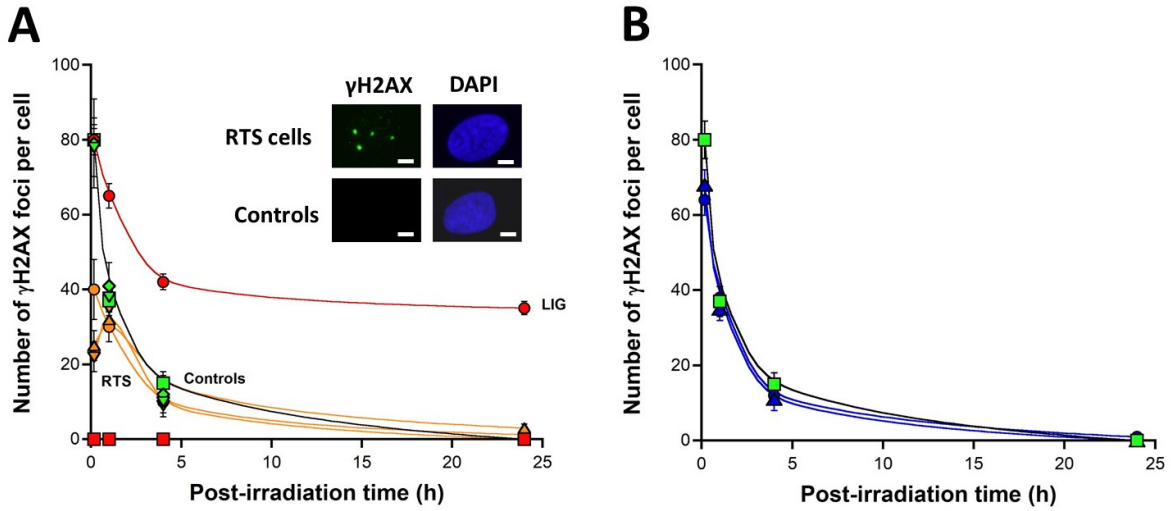

Figure 3. Kinetics of γH2AX foci in RTS fibroblasts**.** *Anti-γH2AX* immunofluorescence was applied to (**A**): the radioresistant controls (green symbols: 1BR3, squares; MRC5, diamonds; Hs27, inverted triangles), the hyper-radiosensitive *LIG4*-mutated 180BR (red circles), and the three RTS (orange symbols: 81CLB, circles; AG17524, triangles; AG18371 inverted triangles) fibroblast cell lines and to (**B**): 2 fibroblast cell lines from parents of RTS patients (blue symbols: AG18466, circles and AG18373, triangles) in addition to the radioresistant 1BR3 controls (green squares). The number of γH2AX

foci was plotted against the post-irradiation time. Each plot represents the mean ± SEM of three replicates. For clarity, only the 1BR3 data, the 81CLB, AG17524, and AG18371 data, the 180BR data, and the AG18466 and AG18373 data were fitted. Data were fitted to the Bodgi's formula [58]. The insert in panel A shows a representative example of γH2AX foci assessed 24 h post-irradiation in one RTS fibroblast cell line (81CLB) and one radioresistant control (1BR3), with the corresponding DAPI counterstaining. The white bar corresponds to 5 μm.

At 24 h post-irradiation, the RTS fibroblasts showed a similar number of γH2AX foci as the radioresistant controls ($p > 0.3$), suggesting that the repair rate of DSB recognized by NHEJ can be considered normal at this time. After 24 h post-irradiation, the number of DSB recognized by NHEJ and remaining unrepaired was similar in the radioresistant control and in the RTS patients' cells (Figure 3A). Together, these data suggest a lack of DSB recognition by NHEJ that was not accompanied by a gross DSB repair defect of DSB recognized by NHEJ as in the *LIG4*-mutated cells. The fibroblasts from the parents of the RTS patients showed γH2AX foci kinetics similar to those observed in radioresistant controls ($p > 0.8$) (Figure 3B).

3.4. Abnormal Number of pATM Foci after Irradiation in RTS Fibroblasts

According to the RIANS model, since the formation of γH2AX foci is ATM-dependent, a low number of early γH2AX foci suggests that the diffusion of ATM in the nucleus is delayed. Once in the nucleus, the ATM monomers reassociate after the DSB repair process to form ATM dimers, easily quantifiable as nuclear foci by immunofluorescence with the specific antibodies of the auto-phosphorylated forms of ATM (pATM) [43]. The number of pATM foci assessed after 2 Gy was 40 ± 4 in the radioresistant controls, in agreement with previous studies (Figure 4A). In the RTS fibroblasts, the number of pATM foci per cell observed 10 min post-irradiation was significantly lower than that in control fibroblasts (81CLB: 22 ± 6; AG17524: 19 ± 4; AG18371: 19 ± 3; $p < 0.001$). A similar conclusion was reached with pATM foci data assessed at 1 h post-irradiation ($p < 0.05$). In agreement with the literature, the *ATM*-mutated fibroblasts did not show pATM foci while the *LIG4*-mutated showed normal pATM foci kinetics. These data suggest that the RTS fibroblasts elicited abnormal ATM nuclear kinase activity in response to radiation (Figure 4A). Similar to γH2AX foci, the fibroblasts derived from the parents of the RTS patients elicited normal pATM foci kinetics ($p > 0.7$) (Figure 4B).

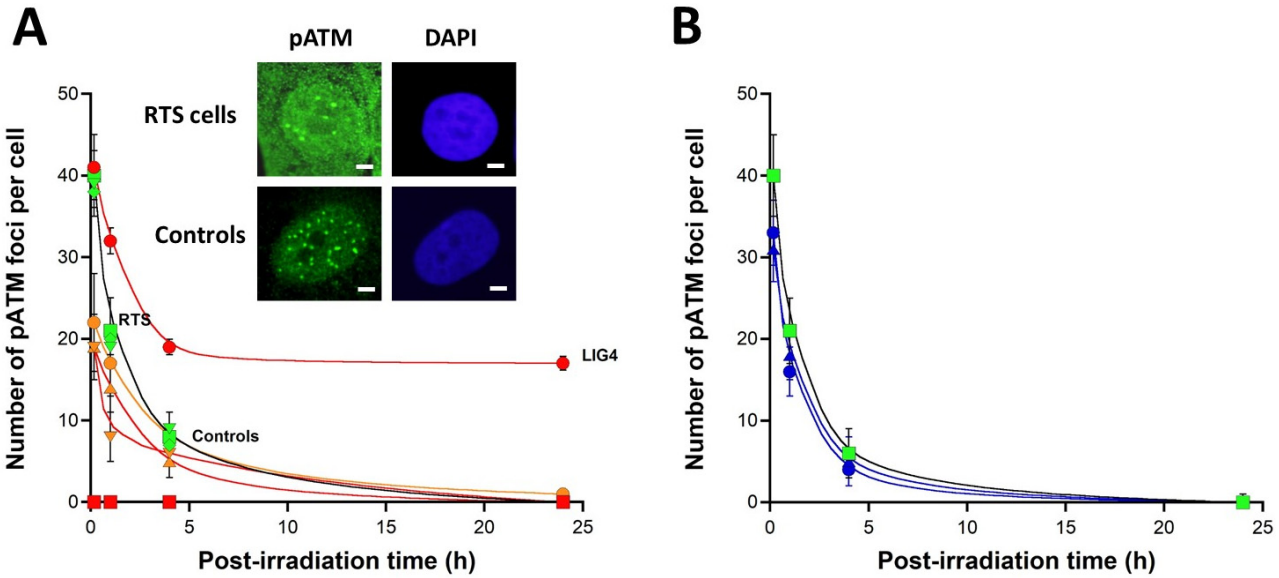

Figure 4. Kinetics of pATM foci in RTS fibroblasts. *Anti-pATM* immunofluorescence was applied to (**A**): the radioresistant controls (green symbols: 1BR3, squares; MRC5, diamonds; Hs27, inverted triangles), the hyper-radiosensitive *LIG4*-mutated 180BR (red circles) and the three RTS (orange

symbols: 81CLB, circles; AG17524, triangles; AG18371 inverted triangles) fibroblast cell lines and to (**B**): 2 fibroblast cell lines from parents of RTS patients (blue symbols: AG18466, circles and AG18373, triangles) in addition to the radioresistant 1BR3 controls (green squares). The number of pATM foci was plotted against the post-irradiation time. Each plot represents the mean ± SEM of three replicates. For clarity, only the 1BR3 data, the 81CLB, AG17524, and AG18371 data, the 180BR, and the AG18466 and AG18373 data were fitted. Data were fitted to the Bodgi's formula [58]. The insert in panel A shows a representative example of pATM foci assessed 1 h post-irradiation in one RTS fibroblast cell line (81CLB) and one radioresistant control (1BR3), with the corresponding DAPI counterstaining. The white bar corresponds to 3 μm.

The survival and pATM data from the three fibroblast cell lines were found in full agreement with the correlation established between SF2 and early pATM foci with fibroblasts from different genetic diseases and published recently [45] (Figure 5). Such findings support again the quantitative consistence of our data.

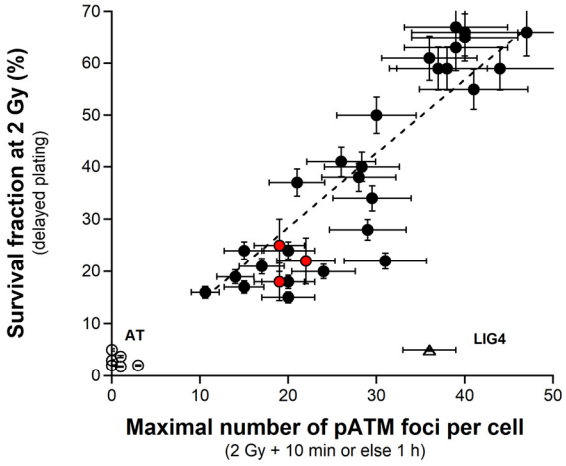

Figure 5. SF2 vs pATMmax relationship. By using historical data published in [45], the SF2 and the corresponding γH2AX foci data assessed 24 h post-irradiation and obtained from 36 COPERNIC cell lines were plotted together (closed black circles). Each point corresponds to the mean ± standard error of the mean (SEM) of 3 independent triplicates, at least. The survival and pATM data from the RTS fibroblast cell lines shown in Figures 1 and 4A were added to the graph (red circles). The best data fit was obtained with the linear law: SF2 (pATMmax) = 1.422 × pATMmax; $r^2 = 0.87$ (dotted line).

3.5. Abnormal Number of MRE11 Foci after Irradiation in RTS Fibroblasts

According to the RIANS model, in addition to the formation of the γH2AX foci, the radiation-induced diffusion of ATM monomers in the nucleus also triggers the phosphorylation of the MRE11 nuclease protein, responsible for its inhibition, that is accompanied by the formation of nuclear MRE11 foci. We investigated therefore the occurrence of MRE11 foci in the RTS fibroblasts. In the radioresistant controls, the MRE11 foci appeared from 2 to 8 h post-irradiation and reached their maximal yield at 4 h (7 ± 2 MRE11 foci per cell), in agreement with previous data (Figure 6A). The shape of the MRE11 foci kinetics of the three fibroblast cell lines appeared to be clearly different from that of the radioresistant controls ($p < 0.01$). For the 81CLB and AG18371 fibroblasts, the maximal number of MRE11 foci was reached at 1 h and decreased up to 0 at 24 h post-irradiation. For the AG17524 fibroblasts, the number of MRE11 increased progressively to reach its maximal value at 24 h post-irradiation. It is noteworthy that, for both *ATM*- and *LIG4*-mutated fibroblasts, the formation of the MRE11 foci was impaired (Figure 6A). Like for γH2AX and pATM foci, the fibroblasts deriving from the parents of the RTS patients elicited normal MRE11 foci kinetics ($p > 0.7$) (Figure 6B).

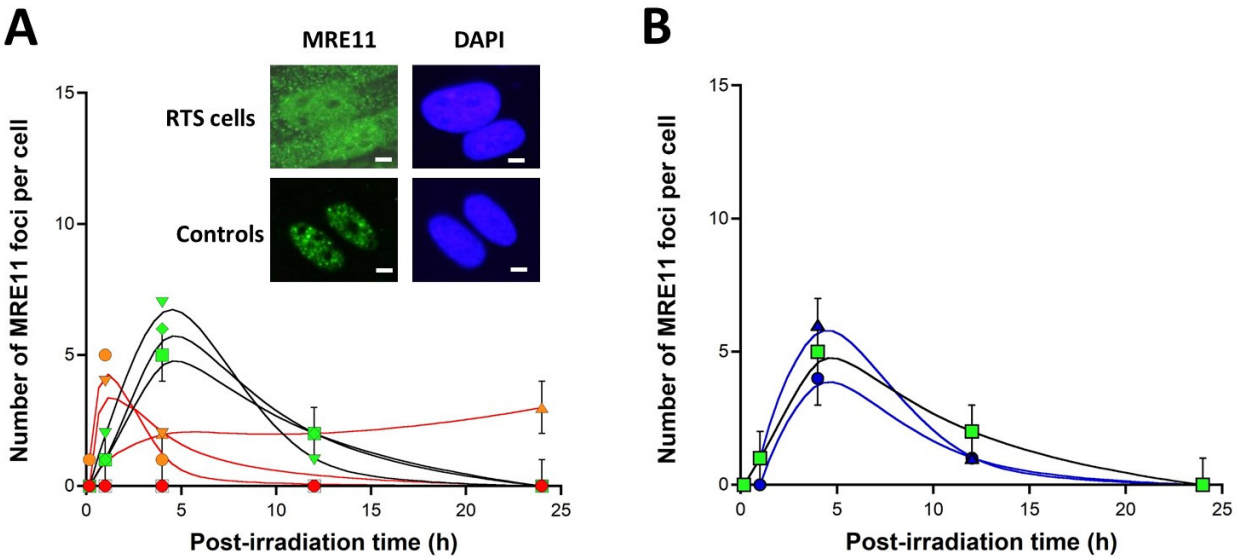

Figure 6. Kinetics of MRE11 foci in RTS fibroblasts. *Anti-MRE11* immunofluorescence was applied to (**A**): the radioresistant controls (green symbols: 1BR3, squares; MRC5, diamonds; Hs27, inverted triangles), the hyper-radiosensitive *ATM*-mutated AT4BI (red squares) and *LIG4*-mutated 180BR (red circles), and the three RTS (orange symbols: 81CLB, circles; AG17524, triangles; AG18371 inverted triangles) fibroblast cell lines and to (**B**): 2 fibroblast cell lines from the parents of RTS patients (blue symbols: AG18466, circles and AG18373, triangles) in addition to the radioresistant 1BR3 controls (green squares). The number of MRE11 foci was plotted against the post-irradiation time. Each plot represents the mean ± SEM of three replicates. Data were fitted to Bodgi's formula [58]. The insert in panel A shows a representative example of MRE11 foci assessed 1 h post-irradiation in one RTS fibroblast cell line (81CLB) and one radioresistant control (1BR3), with the corresponding DAPI counterstaining. The white bar corresponds to 3 μm.

3.6. Subcellular Localization and Expression of the RECQL4 Protein in RTS Fibroblasts

A delayed RIANS is generally caused by the interaction between ATM monomers and some ATM substrates that are overexpressed in the cytoplasm [43]. We therefore examined the existence of potential cytoplasmic ATM-RECQL4 complexes in RTS fibroblasts. To this aim, as a first step, we investigated the expression of the RECQL4 protein in both total and cytoplasmic cell extracts by using immunoblots. By considering the total protein extracts, the level of RECQL4 expression appeared higher in the three fibroblast cell lines than in the radioresistant controls. Interestingly, the cytoplasmic RECQL4 forms were found absent in radioresistant controls, suggesting that the RECQL4 protein is essentially nuclear in these cells, in agreement with the literature (Table 1 and references therein) (Figure 7 and supplementary file). Hence, immunoblots highlighted the existence of abundant cytoplasmic forms of the RECQL4 protein in the three fibroblast cell lines tested. Interestingly, cytoplasmic forms of the RECQL4 proteins also appeared abundant in heterozygous RTS carriers, suggesting that heterozygous *RECQL4* mutations may also lead to over-expressed cytoplasmic RECQL4 proteins (Figure 7).

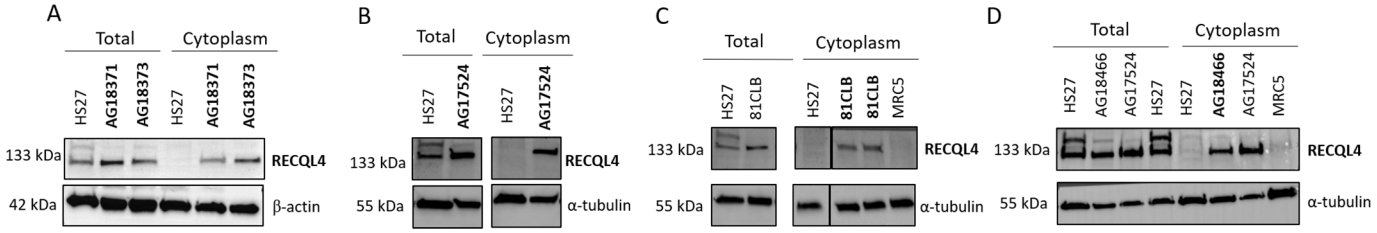

Figure 7. Subcellular localization of the RECQL4 protein in RTS fibroblasts. (**A**–**D**). Anti-*RECQL4* immunoblots with total or cytoplasmic protein extracts of the indicated non-irradiated RTS and control fibroblasts tested in this study.

As a second step, the proximity ligation assay (PLA) was thereafter applied to the three RTS and one radioresistant control fibroblasts (Figure 8). The PLA assay revealed 2–3 times significantly more cytoplasmic ATM-RECQL4 complexes in the RTS fibroblasts ($p < 0.01$) than in radioresistant controls. The irradiation did not significantly influence the number of PLA foci reflecting the ATM-RECQL4 complexes (Figure 8).

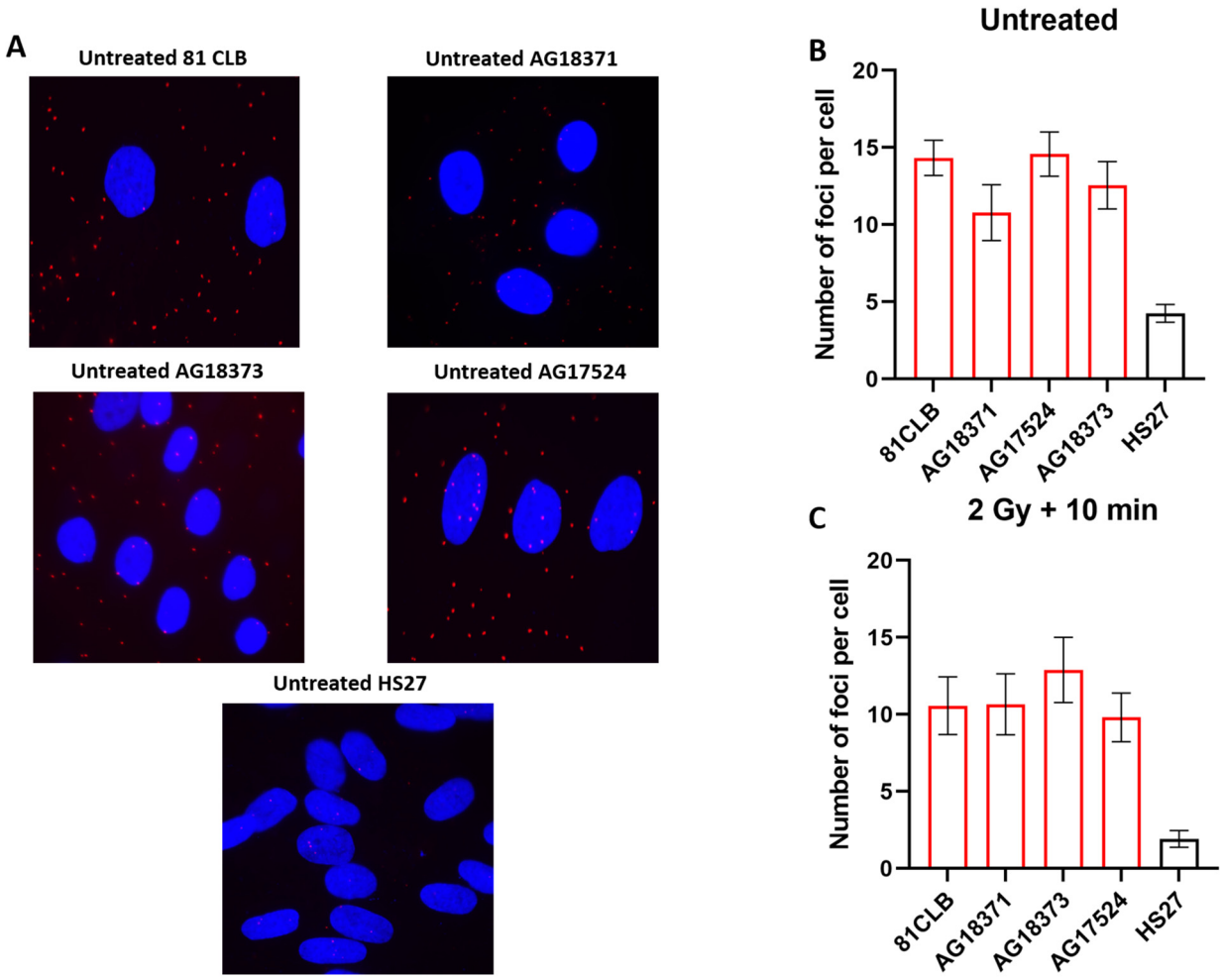

Figure 8. Interaction between ATM and RECQL4 proteins**.** Proximity ligation assay (PLA) was applied to the indicated cell lines. (**A**). Representative PLA images obtained from the indicated RTS and control cells. The nuclei were counterstained with DAPI (blue). The red foci indicate an ATM-RECQL4 protein complex. (**B**,**C**). The average numbers of red foci representing the ATM-RECQL4 protein complexes were scored per 100 cells without irradiation (**B**) or 10 min post-irradiation (**C**). Each data point represents the mean ± SEM of two independent replicates.

3.7. Statin and Bisphosphonate Treatment Protects RTS Fibroblasts from Radiation

The combination of pravastatin and zoledronate treatments (ZOPRA) was shown to accelerate the RIANS and, in some genetic diseases, to decrease the radiosensitivity [35–38]. The ZOPRA treatment was therefore applied to the RTS fibroblasts with micronuclei and early γH2AX and pATM foci. With regard to micronuclei, the ZOPRA treatment significantly reduced the number of residual micronuclei only in the RTS 81CLB fibroblasts.

With regard to the early γH2AX and pATM foci, the ZOPRA treatment significantly increased the number of foci in all three fibroblast cell lines tested (Figure 9). Together, these data suggest that the ZOPRA treatment may protect the RTS fibroblasts against IR by accelerating the RIANS and stimulating the ATM kinase activity in the nucleus, at least partially.

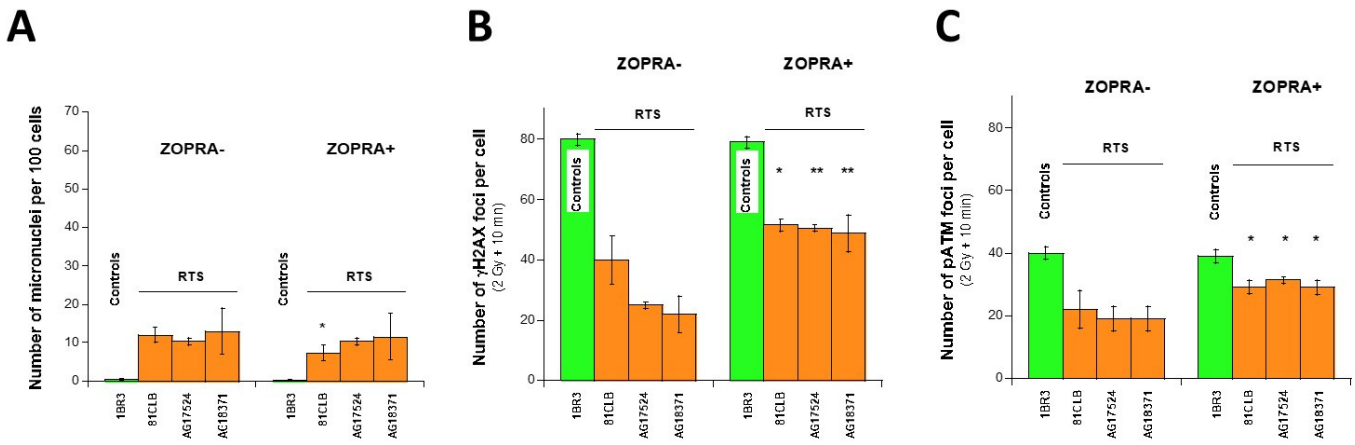

Figure 9. Effect of ZOPRA treatment on RTS fibroblasts**.** Numbers of micronuclei per 100 cells assessed after 2 Gy followed by 24 h post-irradiation (**A**), numbers of γH2AX foci per cell assessed after 2 Gy followed by 10 min post-irradiation (**B**), numbers of pATM foci per cell assessed after 2 Gy followed by 10 min post-irradiation (**C**) in the indicated control and RTS fibroblasts with or without ZOPRA treatment. Data plots represent the mean ± SEM of duplicate experiments. Asterisks represent the statistical differences with untreated cells expressed as *p*-value (1 and 2 asterisks correspond to $p < 0.05$ and $p < 0.01$, respectively).

4. Discussion

4.1. RTS, a Rare Disease Associated with Moderate Radiosensitivity

Our findings suggest that fibroblasts derived from the RTS patients had cellular radiosensitivity, an abnormally high number of radiation-induced micronuclei, and a reduced number of early γH2AX and pATM foci, suggesting a delayed RIANS accompanied by the formation of cytoplasmic ATM-RECQL4 complexes and abnormal kinetics of MRE11 foci. The ZOPRA treatment permitted us to correct, at least partially, the radiosensitivity phenotype observed in the RTS fibroblasts. Since a subset of RTS patients (RTS2 subgroup) are generally at a high risk of cancer, some RTS patients may be exposed to anti-cancer radiotherapy (Table 2 and references therein) but also to chemotherapy drugs, mimicking IR. Furthermore, in order to investigate some clinical features, RTS patients may also be exposed to repeated radiodiagnosis exams. Hence, such irradiating or DNA-breaking acts may raise the question of the potential worsening of some clinical symptoms of RTS patients accelerated by IR or chemotherapy drugs that provide DSB. The radiobiological characterization of the RTS and the role of the RECQL4 protein in the RI DNA damage repair and signaling therefore remain of both medical and scientific interest.

The SF2, the yields of micronuclei, and the number of γH2AX and pATM foci assessed post-irradiation are current biomarkers of radiosensitivity. They are quantitatively linked together [25,34,45]. Particularly, in a recent study, we provided inter-correlations between these biomarkers from a collection of 200 fibroblast cell lines eliciting a large spectrum of radiosensitivity [45]. The data described in this study were in very good agreement with each of the published correlations, therefore supporting their quantitative relevance. As indicated in Table 2, this study is the first work suggesting that skin fibroblasts from RTS patients are radiosensitive, impaired in the DSB recognition step and characterized by a delayed RIANS (Table 2). Interestingly, the cellular radiosensitivity quantified by the cell survival assay in the RTS fibroblasts was in quantitative agreement

with the literature data. Particularly, the radiosensitivity of the RTS fibroblasts was similar to that found in cells from Bloom, Werner, Cockayne, and some xeroderma pigmentosum syndromes, i.e., genetic syndromes caused by mutated helicase [45,59]. However, despite such coherence, since RTS is a very rare syndrome and since few untransformed fibroblast cell lines derived from RTS patients are available, further investigations are needed to generalize our observations to other RTS cases.

4.2. The Radiosensitivity Associated with the RTS and the RIANS Model

How can we explain the level of radiosensitivity observed in the RTS cells? By considering the helicase function of the RECQL4 protein, it appeared natural to directly explain the clinical features specific to the RTS by impaired DNA helicase activity. Besides, the RECQL4 protein has been found to be involved in the choice between the NHEJ and the HR and in the signaling and repair of DSB, the key-damage induced by RI [11,20–24,60]. However, the fibroblasts used in the present study were quiescent. Hence, the impact of the HR on the RI lethal effect was likely to be negligible. Secondly, the cellular models used in the pre-cited studies are tumors that were transformed by sophisticated vectors to over-express the wild-type or the mutated *RECQL4* gene [11,20–24,60]. However, even if an impaired helicase (whose function can be redundant) may explain the significant but moderate radiosensitivity observed in RTS cells, it must be stressed that the cytoplasmic expression of *RECQL4* was systematically higher in the *RECQL4*-mutated fibroblasts than in the radioresistant controls. Lastly, no combination of statins and bisphosphonates was shown to influence DNA helicase activity while the ZOPRA treatment may complement the radiosensitivity phenotype of the three RTS cell lines tested, at least partially: the radiosensitivity associated with the RTS suggests a more complex model.

In the framework of the RIANS model, the oxidative stress produced by IR triggers the formation of DNA damage in the nucleus (notably the DSB) and the monomerization of the ATM dimers (more abundant in the cytoplasm). The ATM monomers diffuse in the nucleus and trigger the recognition of DSB by the NHEJ pathway via the phosphorylation of H2AX by ATM. This scenario corresponds to the radioresistance (so-called group I, in the frame of RIANS model). In the case of delayed RIANS (group II, in the framework of the RIANS model), the ATM monomers are sequestrated in the cytoplasm by over-expressed ATM substrates, called X-proteins. Group II cells show significant but moderate radiosensitivity and are more susceptible to transformation, similar to the RTS cells. Conversely, any acceleration of the RIANS, such as that induced by ZOPRA, may render cells more radioresistant [43]. The X-proteins should therefore reach two major requirements: (1) be overexpressed in the cytoplasm; (2) associate with and/or be phosphorylated by ATM. While we observed abundant cytoplasmic forms of RECQL4 in the three RTS fibroblast cell lines tested here, can the RECQL4 protein be an X-protein in the framework of the RIANS model? Kim et al. have shown that the ATM kinase preferentially phosphorylates the SQ/TQ domains [61]. Interestingly, the RECQL4 protein has five SQ domains (including Ser27 situated in the SLD2 domain and Ser217, Ser326, and Ser 611 situated in the DEAD domain of the core helicase domain) [62]. The PLA data clearly suggested that ATM and RECQL4 preferentially interact in the cytoplasm, which is likely to cause a delay in the RIANS and therefore an alteration of the DSB recognition by the NHEJ pathway (Figure 10). Hence, by considering both the impaired helicase activity but also the role of ATM substrates as X-proteins, mutations of the RECQL4 protein may be linked to an abnormal response to IR. However, further investigations are needed to identify the molecular and cellular role of the phosphorylation of RECQL4 by ATM in quiescent normal and RTS fibroblasts.

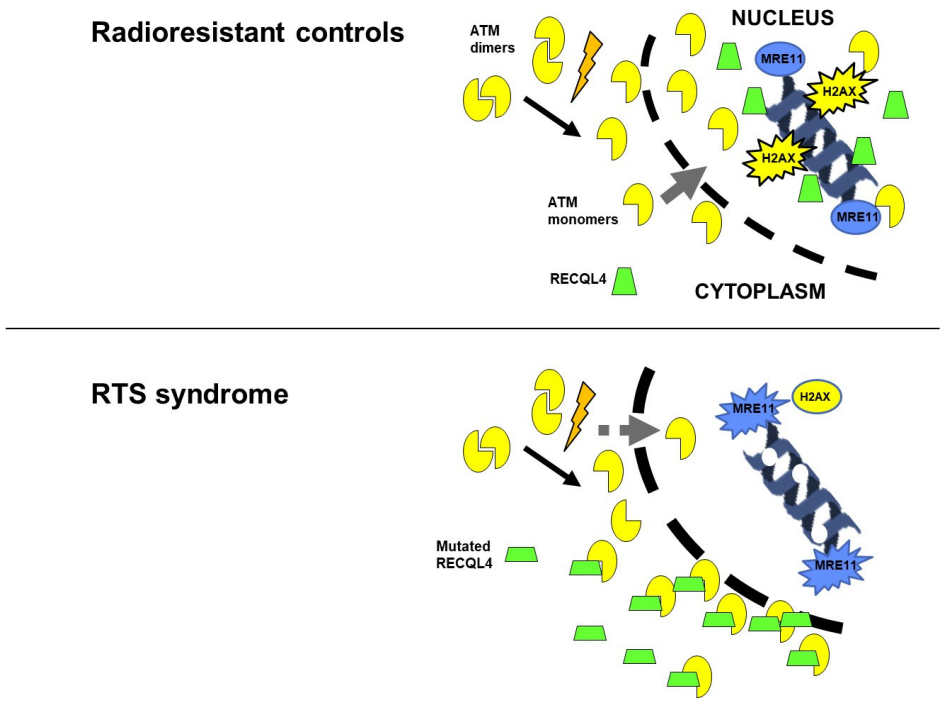

Figure 10. The RTS and the RIANS model**.** Schematic illustration of the RIANS model for the radioresistant and the RTS cells. The IR-induced ATM monomers diffuse in the nucleus, in which they trigger the DSB repair pathway by phosphorylating H2AX (activation of NHEJ) and MRE11 (inhibition of the nuclease activity). In the RTS cells, RECQL4 mutations lead to impaired cytoplasmic localization and/or overexpression of the RECQL4 protein, which results in more ATM-RECQL4 complexes: a significant delay of RIANS occurs with a lack of DSB recognition and repair and increased MRE11 activity. This delay of RIANS may be alleviated by ZOPRA treatment.

5. Conclusions

Our findings indicate that the radiosensitivity and the sensitivity to DNA breaking agents associated with RTS may be caused by an overexpression of some cytoplasmic RECQL4 helicase forms that sequester ATM monomers in the cytoplasm, which leads to a delayed RIANS, impaired DSB recognition, and high genomic instability. Further experiments are required to better quantify the risks caused by radiodiagnosis, radiotherapy or chemotherapy in the healthy tissues of RTS patients and to investigate whether statins, bisphosphonates, and/or anti-oxidative drugs may provide efficient radioprotection.

Supplementary Materials: The following supporting information can be downloaded at: https://www.mdpi.com/article/10.3390/radiation3010002/s1, supplementary file is the full western blots.

Author Contributions: The authors of this manuscript have contributed in the following ways: Conceptualization, J.A.-C., M.N., M.B., N.F.; data acquisition and methodology, J.A.-C., M.M., L.S., A.G., L.E.N., J.R.-V., M.M., E.B., B.A., N.C.; data analysis, J.A.-C., M.N., B.A., N.C., M.B., N.F.; writing and original draft preparation, J.A.-C., M.N., M.B., N.F.; writing, reviewing and editing, all authors; project administration, and funding acquisition, N.F. All authors have read and agreed to the published version of the manuscript.

Funding: This work was supported by the Commissariat General à l'Investissement (Programmes Investissement d'avenir—INDIRA project) and the National Space Agency (CNES)—ICARE project.

Institutional Review Board Statement: As already mentioned in the Materials and Methods, this study was performed with human fibroblast cell lines that belong to the COPERNIC collection of the laboratory that has been approved by the regional Ethical Committee. Cell lines were declared under the numbers DC2008-585, DC2011-1437, and DC2021-3957 to the Ministry of Research.

Informed Consent Statement: All anonymous donors of the COPERNIC collection mentioned above were informed and signed consent according to the ethics and regulatory recommendations, notably for their consent to participate and for publication of anonymous data.

Data Availability Statement: All data can be provided upon reasonable request.

Conflicts of Interest: N.F. reports the following related patents: FR3040178A1, FR3040179A1, WO2017098190A1, EP3685163A. The authors declare no conflict of interest. The funders had no role in the design of the study; in the collection, analyses, or interpretation of data; in the writing of the manuscript, or in the decision to publish the results.

References

1. Rothmund, A. Uber cataracten in Verbindung mit einer eigentumlichen Hautdegeneration. *Arch Klin. Ophthalmol.* **1868**, *14*, 4159–4182.
2. Thomson, M.S. Poikiloderma Congenitale. *Br. J. Dermatol.* **1936**, *48*, 4221–4234.
3. Taylor, W.B. Rothmund's syndrome—Thomson's syndrome. *Arch. Dermatol.* **1957**, *75*, 75236–75244.
4. Larizza, L.; Roversi, G.; Volpi, L. Rothmund-Thomson syndrome. *Orphanet J. Rare Dis.* **2010**, *5*, 2.
5. Wang, L.L.; Levy, M.L.; Lewis, R.A.; Chintagumpala, M.M.; Lev, D.; Rogers, M.; Plon, S.E. Clinical manifestations in a cohort of 41 Rothmund-Thomson syndrome patients. *Am. J. Med. Genet.* **2001**, *102*, 11–17.
6. De Oliveira, K.M.; Silva, R.A.; Carvalho, F.K.; Silva, L.A.; Nelson-Filho, P.; Queiroz, A.M. Clinical findings, dental treatment, and improvement in quality of life for a child with Rothmund-Thomson syndrome. *Contemp. Clin. Dent.* **2016**, *7*, 240–242.
7. Miranda, A.F.; Rivera-Monge, M.D.; Farias, C.C. Rothmund-Thomson syndrome and ocular surface findings: Case reports and review of the literature. *Arq. Bras. Oftalmol.* **2016**, *79*, 186–188.
8. Lu, L.; Jin, W.; Wang, L.L. Aging in Rothmund-Thomson syndrome and related RECQL4 genetic disorders. *Ageing Res. Rev.* **2017**, *33*, 30–35.
9. Hussain, M.; Krishnamurthy, S.; Patel, J.; Kim, E.; Baptiste, B.A.; Croteau, D.L.; Bohr, V.A. Skin Abnormalities in Disorders with DNA Repair Defects, Premature Aging, and Mitochondrial Dysfunction. *J. Investig. Dermatol.* **2021**, *141*, (Suppl. 4), 968–975.
10. Kitao, S.; Shimamoto, A.; Goto, M.; Miller, R.W.; Smithson, W.A.; Lindor, N.M.; Furuichi, Y. Mutations in RECQL4 cause a subset of cases of Rothmund-Thomson syndrome. *Nat. Genet.* **1999**, *22*, 82–84.
11. Xu, X.; Chang, C.W.; Li, M.; Liu, C.; Liu, Y. Molecular Mechanisms of the RECQ4 Pathogenic Mutations. *Front. Mol. Biosci.* **2021**, *8*, 791194.
12. Zirn, B.; Bernbeck, U.; Alt, K.; Oeffner, F.; Gerhardinger, A.; Has, C. Rothmund-Thomson syndrome type 1 caused by biallelic ANAPC1 gene mutations. *Ski. Health Dis.* **2021**, *1*, e122021.
13. Siitonen, H.A.; Kopra, O.; Kaariainen, H.; Haravuori, H.; Winter, R.M.; Saamanen, A.M.; Peltonen, L.; Kestila, M. Molecular defect of RAPADILINO syndrome expands the phenotype spectrum of RECQL diseases. *Hum. Mol. Genet.* **2003**, *12*, 2837–2844.
14. Van Maldergem, L.; Siitonen, H.A.; Jalkh, N.; Chouery, E.; De Roy, M.; Delague, V.; Muenke, M.; Jabs, E.W.; Cai, J.; Wang, L.L.; et al. Revisiting the craniosynostosis-radial ray hypoplasia association: Baller-Gerold syndrome caused by mutations in the RECQL4 gene. *J. Med. Genet.* **2006**, *43*, 148–152.
15. Brosh, R.M., Jr.; Bohr, V.A. Human premature aging, DNA repair and RecQ helicases. *Nucleic Acids Res.* **2007**, *35*, 7527–7544.
16. Mohaghegh, P.; Hickson, I.D. Premature aging in RecQ helicase-deficient human syndromes. *Int. J. Biochem. Cell Biol.* **2002**, *34*, 1496–1501.
17. Arora, H.; Chacon, A.H.; Choudhary, S.; McLeod, M.P.; Meshkov, L.; Nouri, K.; Izakovic, J. Bloom syndrome. *Int. J. Derm.* **2014**, *53*, 798–802.
18. Ozgenc, A.; Loeb, L.A. Werner Syndrome, aging and cancer. *Genome Dyn.* **2006**, *1*, 206–217.
19. Kaneko, H.; Takemoto, M.; Murakami, H.; Ihara, K.; Kosaki, R.; Motegi, S.I.; Taniguchi, A.; Matsuo, M.; Yamazaki, N.; Nishigori, C.; et al. Rothmund-Thomson syndrome investigated by two nationwide surveys in Japan. *Pediatr. Int.* **2022**, *64*, e15120.
20. Mo, D.; Zhao, Y.; Balajee, A.S. Human RecQL4 helicase plays multifaceted roles in the genomic stability of normal and cancer cells. *Cancer Lett.* **2018**, *413*, 1–10.
21. Shamanna, R.A.; Singh, D.K.; Lu, H.; Mirey, G.; Keijzers, G.; Salles, B.; Croteau, D.L.; Bohr, V.A. RECQ helicase RECQL4 participates in non-homologous end joining and interacts with the Ku complex. *Carcinogenesis* **2014**, *35*, 2415–2424.
22. Lu, H.; Shamanna, R.A.; de Freitas, J.K.; Okur, M.; Khadka, P.; Kulikowicz, T.; Holland, P.P.; Tian, J.; Croteau, D.L.; Davis, A.J.; et al. Cell cycle-dependent phosphorylation regulates RECQL4 pathway choice and ubiquitination in DNA double-strand break repair. *Nat. Commun.* **2017**, *8*, 2039.
23. Lu, H.; Shamanna, R.A.; Keijzers, G.; Anand, R.; Rasmussen, L.J.; Cejka, P.; Croteau, D.L.; Bohr, V.A. RECQL4 Promotes DNA End Resection in Repair of DNA Double-Strand Breaks. *Cell Rep.* **2016**, *16*, 161–173.
24. Lu, H.; Guan, J.; Wang, S.Y.; Li, G.M.; Bohr, V.A.; Davis, A.J. DNA-PKcs-dependent phosphorylation of RECQL4 promotes NHEJ by stabilizing the NHEJ machinery at DNA double-strand breaks. *Nucleic Acids Res.* **2022**, *50*, 5635–5651.
25. Foray, N.; Bourguignon, M.; Hamada, N. Individual response to ionizing radiation. *Mutat. Res. Rev.* **2016**, *770*, 369–386.

26. ASN. Arrêté du 8 février 2019 portant homologation de la décision n° 2019-DC-0660 de l'Autorité de sûreté nucléaire du 15 janvier 2019 fixant les obligations d'assurance de la qualité en imagerie médicale mettant en œuvre des rayonnements ionisants. *JORF* **2019,** doi:JORFTEXT000038121063.
27. Smith, P.J.; Paterson, M.C. Enhanced radiosensitivity and defective DNA repair in cultured fibroblasts derived from Rothmund Thomson syndrome patients. *Mutat. Res.* **1982**, *94*, 213–228.
28. Shinya, A.; Nishigori, C.; Moriwaki, S.; Takebe, H.; Kubota, M.; Ogino, A.; Imamura, S. A case of Rothmund-Thomson syndrome with reduced DNA repair capacity. *Arch. Derm.* **1993**, *129*, 332–336.
29. Varughese, M.; Leavey, P.; Smith, P.; Sneath, R.; Breatnach, F.; O'Meara, A. Osteogenic sarcoma and Rothmund Thomson syndrome. *J. Cancer Res. Clin. Oncol.* **1992**, *118*, 389–390.
30. Jin, W.; Liu, H.; Zhang, Y.; Otta, S.K.; Plon, S.E.; Wang, L.L. Sensitivity of RECQL4-deficient fibroblasts from Rothmund-Thomson syndrome patients to genotoxic agents. *Hum. Genet.* **2008**, *123*, 643–653.
31. Kerr, B.; Ashcroft, G.S.; Scott, D.; Horan, M.A.; Ferguson, M.W.; Donnai, D. Rothmund-Thomson syndrome: Two case reports show heterogeneous cutaneous abnormalities, an association with genetically programmed ageing changes, and increased chromosomal radiosensitivity. *J. Med. Genet.* **1996**, *33*, 928–934.
32. Borg, M.F.; Olver, I.N.; Hill, M.P. Rothmund-Thomson syndrome and tolerance of chemoradiotherapy. *Australas. Radiol.* **1998**, *42*, 216–218.
33. Dahele, M.R.; Benton, E.C.; Hennessy, A.; MacDougall, R.H.; Price, A.; Mitchell, R.; Watson, J. A patient with Rothmund-Thomson syndrome and tongue cancer--experience of radiation toxicity. *Clin. Oncol. (R. Coll Radiol.)* **2004**, *16*, 371–372.
34. Averbeck, D.; Candeias, S.; Chandna, S.; Foray, N.; Friedl, A.A.; Haghdoost, S.; Jeggo, P.A.; Lumniczky, K.; Paris, F.; Quintens, R.; et al. Establishing mechanisms affecting the individual response to ionizing radiation. *Int. J. Radiat. Biol.* **2020**, *96*, 297–323.
35. Ferlazzo, M.L.; Sonzogni, L.; Granzotto, A.; Bodgi, L.; Lartin, O.; Devic, C.; Vogin, G.; Pereira, S.; Foray, N. Mutations of the Huntington's Disease Protein Impact on the ATM-Dependent Signaling and Repair Pathways of the Radiation-Induced DNA Double-Strand Breaks: Corrective Effect of Statins and Bisphosphonates. *Mol. Neurobiol.* **2014**, *49*, 1200–1211.
36. Ferlazzo, M.L.; Bach-Tobdji, M.K.E.; Djerad, A.; Sonzogni, L.; Burlet, S.F.; Devic, C.; Granzotto, A.; Bodgi, L.; Djeffal-Kerrar, A.; Foray, N. Radiobiological characterization of tuberous sclerosis: A delay in the nucleo-shuttling of ATM may be responsible for radiosensitivity. *Mol. Neurobiol.* **2017**, 55, 4973–4983.
37. Combemale, P.; Sonzogni, L.; Devic, C.; Bencokova, Z.; Ferlazzo, M.L.; Granzotto, A.; Burlet, S.F.; Pinson, S.; Amini-Adle, M.; Al-Choboq, J.; et al. Individual response to radiation of individuals with neurofibromatosis type I: Role of the ATM protein and influence of statins and bisphosphonates. *Mol. Neurobiol.* **2021**, *59*, 556–573.
38. Ferlazzo, M.; Berthel, E.; Granzotto, A.; Devic, C.; Sonzogni, L.; Bachelet, J.T.; Pereira, S.; Bourguignon, M.; Sarasin, A.; Mezzina, M.; et al. Some mutations in the xeroderma pigmentosum D gene may lead to moderate but significant radiosensitivity associated with a delayed radiation-induced ATM nuclear localization. *Int. J. Radiat. Biol.* **2019**, *96*, 394–410.
39. Granzotto, A.; Benadjaoud, M.A.; Vogin, G.; Devic, C.; Ferlazzo, M.L.; Bodgi, L.; Pereira, S.; Sonzogni, L.; Forcheron, F.; Viau, M.; et al. Influence of Nucleoshuttling of the ATM Protein in the Healthy Tissues Response to Radiation Therapy: Toward a Molecular Classification of Human Radiosensitivity. *Int. J. Radiat. Oncol. Biol. Phys.* **2016**, *94*, 450–460.
40. Belkacemi, Y.; Colson-Durand, L.; Granzotto, A.; Husheng, S.; To, N.H.; Majdoul, S.; Guet, S.; Herve, M.L.; Fonteneau, G.; Diana, C.; et al. The Henri Mondor Procedure of Morbidity and Mortality Review Meetings: Prospective Registration of Clinical, Dosimetric, and Individual Radiosensitivity Data of Patients with Severe Radiation Toxicity. *Int. J. Radiat. Oncol. Biol. Phys.* **2016**, *96*, 629–636.
41. Pereira, S.; Bodgi, L.; Duclos, M.; Canet, A.; Ferlazzo, M.L.; Devic, C.; Granzotto, A.; Deneuve, S.; Vogin, G.; Foray, N. Fast and binary assay for predicting radiosensitivity based on the nucleoshuttling of ATM protein: Development, validation and performances. *Int. J. Radiat. Oncol. Biol. Phys.* **2018**, *100*, 353–360.
42. Vogin, G.; Bastogne, T.; Bodgi, L.; Gillet-Daubin, J.; Canet, A.; Pereira, S.; Foray, N. The Phosphorylated ATM Immunofluorescence Assay: A High-performance Radiosensitivity Assay to Predict Postradiation Therapy Overreactions. *Int. J. Radiat. Oncol. Biol. Phys.* **2018**, *101*, 690–693.
43. Berthel, E.; Foray, N.; Ferlazzo, M.L. The Nucleoshuttling of the ATM Protein: A Unified Model to Describe the Individual Response to High- and Low-Dose of Radiation? *Cancers* **2019**, *11*, 905.
44. Bodgi, L.; Foray, N. The nucleo-shuttling of the ATM protein as a basis for a novel theory of radiation response: Resolution of the linear-quadratic model. *Int. J. Radiat. Biol.* **2016**, *92*, 117–131.
45. Le Reun, E.; Bodgi, L.; Granzotto, A.; Sonzogni, L.; Ferlazzo, M.L.; Al-Choboq, J.; El-Nachef, L.; Restier-Verlet, J.; Berthel, E.; Devic, C.;et al. Quantitative correlations between radiosensitivity biomarkers show that the ATM protein kinase is strongly involved in the radiotoxicities observed after radiotherapy. *Int. J. Mol. Sci.* **2022**, 23, 10434.
46. Moulay Lakhdar, I.; Ferlazzo, M.L.; Al Choboq, J.; Berthel, E.; Sonzogni, L.; Devic, C.; Granzotto, A.; Thariat, J.; Foray, N. Fibroblasts from Retinoblastoma Patients Show Radiosensitivity Linked to Abnormal Localization of the ATM Protein. *Curr. Eye Res.* **2020**, *46*, 546–557.
47. Joubert, A.; Zimmerman, K.M.; Bencokova, Z.; Gastaldo, J.; Rénier, W.; Chavaudra, N.; Favaudon, V.; Arlett, C.; Foray, N. DNA double-strand break repair defects in syndromes associated with acute radiation response: At least two different assays to predict intrinsic radiosensitivity? *Int. J. Radiat. Biol.* **2008**, *84*, 107–125.

48. Al-Choboq, J.; Ferlazzo, M.L.; Sonzogni, L.; Granzotto, A.; El-Nachef, L.; Maalouf, M.; Berthel, E.; Foray, N. Usher Syndrome Belongs to the Genetic Diseases Associated with Radiosensitivity: Influence of the ATM Protein Kinase. *Int. J. Mol. Sci.***2022**, *23*, 1570.
49. Bachelet, J.M.; Al-Choboq, J.; Granzotto, A.; Ferlazzo, M.L.; Sonzogni, L.; Berthel, E.; Devic, C.; Foray, N. Radiobiological characterization of skin fibroblasts from a young patient suffering from the Immunodeficiency Centromeric instability Facial anomalies type 1 (ICF1) syndrome. *Arch. Med. Clin. Case Rep.* **2022**, *in press*.
50. Bachelet, J.T.; Granzotto, A.; Ferlazzo, M.; Sonzogni, L.; Berthel, E.; Devic, C.; Foray, N. First Radiobiological Characterization of Skin and Bone Cells from A Patient Suffering from the PI3KCA-Related Overgrowth Spectrum (PROS) Syndrome. *Arch. Med. Clin. Case Rep.* **2020**, *4*, 1052–1066.
51. Bachelet, J.T.; Granzotto, A.; Ferlazzo, M.; Sonzogni, L.; Berthel, E.; Devic, C.; Foray, N. First radiobiological characterization of the McCune-Albright syndrome: Influence of the ATM protein and effect of statins + bisphosphonates treatment. *Int. J. Radiat. Biol.* **2021**, *97*, 317–328.
52. Foray, N.; Priestley, A.; Alsbeih, G.; Badie, C.; Capulas, E.P.; Arlett, C.F.; Malaise, E.P. Hypersensitivity of ataxia telangiectasia fibroblasts to ionizing radiation is associated with a repair deficiency of DNA double-strand breaks. *Int. J. Radiat. Biol.* **1997**, *72*, 271–283.
53. Varela, I.; Pereira, S.; Ugalde, A.P.; Navarro, C.L.; Suarez, M.F.; Cau, P.; Cadinanos, J.; Osorio, F.G.; Foray, N.; Cobo, J.; et al. Combined treatment with statins and aminobisphosphonates extends longevity in a mouse model of human premature aging. *Nat. Med.* **2008**, *14*, 767–772.
54. Fertil, B.; Malaise, E.P. Inherent cellular radiosensitivity as a basic concept for human tumor radiotherapy. *Int. J. Radiat. Oncol. Biol. Phys.* **1981**, *7*, 621–629.
55. Grote, S.J.; Joshi, G.P.; Revell, S.H.; Shaw, C.A. Observations of radiation-induced chromosome fragment loss in live mammalian cells in culture, and its effect on colony-forming ability. *Int. J. Radiat. Biol. Relat. Stud. Phys. Chem. Med.* **1981**, *39*, 395–408.
56. Fenech, M. The in vitro micronucleus technique. *Mutat. Res.* **2000**, *455*, 81–95.
57. Ristic, M.; Brockly, F.; Piechaczyk, M.; Bossis, G. Detection of Protein-Protein Interactions and Posttranslational Modifications Using the Proximity Ligation Assay: Application to the Study of the SUMO Pathway. *Methods Mol. Biol.* **2016**, *1449*, 279–290.
58. Bodgi, L.; Granzotto, A.; Devic, C.; Vogin, G.; Lesne, A.; Bottollier-Depois, J.F.; Victor, J.M.; Maalouf, M.; Fares, G.; Foray, N. A single formula to describe radiation-induced protein relocalization: Towards a mathematical definition of individual radiosensitivity. *J. Theor. Biol.* **2013**, *333*, 135–145.
59. Deschavanne, P.J.; Fertil, B. A review of human cell radiosensitivity in vitro. *Int. J. Radiat. Oncol. Biol. Phys.* **1996**, *34*, 251–266.
60. El Nachef, L.; Berthel, E.; Ferlazzo, M.L.; Le Reun, E.; Al-Choboq, J.; Restier-Verlet, J.; Granzotto, A.; Sonzogni, L.; Bourguignon, M.; Foray, N. Cancer and Radiosensitivity Syndromes: Is Impaired Nuclear ATM Kinase Activity the Primum Movens? *Cancers* **2022**, *14*, 6141.
61. Kim, S.T.; Lim, D.S.; Canman, C.E.; Kastan, M.B. Substrate specificities and identification of putative substrates of ATM kinase family members. *J. Biol. Chem.* **1999,** *274*, 37538–37543.
62. Lu, H.; Davis, A.J. Human RecQ Helicases in DNA Double-Strand Break Repair. *Front. Cell Dev. Biol.* **2021**, *9*, 640755.